Journal of Biomaterials Science, Polymer Edition

ISSN: 0920-5063 (Print) 1568-5624 (Online) Journal homepage: http://www.tandfonline.com/loi/tbsp20

Synthesis, characterization, and in vitro evaluation of targeted gold nanoshelled poly(D,L-lactide-co-glycolide) nanoparticles carrying anti p53 antibody as a theranostic agent for ultrasound contrast imaging and photothermal therapy

Li Xu, Caifeng Wan, Jing Du, Hongli Li, Xuesong Liu, Hong Yang & Fenghua Li

To cite this article: Li Xu, Caifeng Wan, Jing Du, Hongli Li, Xuesong Liu, Hong Yang & Fenghua Li (2017): Synthesis, characterization, and in vitro evaluation of targeted gold nanoshelled poly(D,L-lactide-co-glycolide) nanoparticles carrying anti p53 antibody as a theranostic agent for ultrasound contrast imaging and photothermal therapy, Journal of Biomaterials Science, Polymer Edition, DOI: 10.1080/09205063.2016.1277828

To link to this article: http://dx.doi.org/10.1080/09205063.2016.1277828

Accepted author version posted online: 03 Jan 2017.

Publisher: Taylor & Francis

Journal: *Journal of Biomaterials Science, Polymer Edition*

DOI: http://dx.doi.org/10.1080/09205063.2016.1277828

Synthesis, characterization, and in vitro evaluation of targeted gold nanoshelled poly(D,L-lactide-co-glycolide) nanoparticles carrying anti p53 antibody as a theranostic agent for ultrasound contrast imaging and photothermal therapy

Li Xu[a#], Caifeng, Wan [a#], Jing Du[a], Hongli, Li[a], Xuesong, Liu[a], Hong Yang[b]* and Fenghua, Li[a]*

[a] *Department of Ultrasound, Renji Hospital, School of Medicine, Shanghai Jiao Tong University, Shanghai, 200127,PR China*

[b] *The Key Laboratory of Resource Chemistry of Ministry of Education and the Shanghai Key Laboratory of the Rare Earth Functional Materials, Department of Chemistry, College of Life and Environmental Science, Shanghai Normal University, Shanghai, 200234, PR China*

*Corresponding authors.

[#] *These two authors contributed equally to this work.*

1.Professor Fenghua Li, Department of Ultrasound, Renji Hospital, School of Medicine, Shanghai Jiao Tong University, 1630 Dongfang Road, Shanghai 200127, P.R. China E-mail: fenghua-li@163.com. Tel: 021-68383371

2.Professor Hong Yang, The Key Laboratory of Resource Chemistry of Ministry of Education and the Shanghai Key Laboratory of the Rare Earth Functional Materials, Department of Chemistry, College of Life and Environmental Science, Shanghai Normal University, Shanghai 200234, PR China. E-mail: yanghong@shnu.edu.cn. Tel：021-64328981

Synthesis, characterization, and in vitro evaluation of targeted gold nanoshelled poly(D,L-lactide-co-glycolide) nanoparticles carrying anti p53 antibody as a theranostic agent for ultrasound contrast imaging and photothermal therapy

Breast cancer is the leading cause of cancer-related deaths in women and earlier detection can substantially reduce deaths from breast cancer. Polymers with targeted ligands are widely used in the field of molecular ultrasound imaging and targeted tumor therapy. In our study, the nanotheranostic agent was fabricated through filling perfluoropropane (C_3F_8) into poly(D,L-lactic-co-glycolic acid) nanoparticles (PLGA NPs), followed by the formation of gold nanoshell on the surface, then conjugated with anti p53 antibody which has high specificity with the p53 protein overexpressing in breast cancer. The average diameter of the gold nanoshelled PLGA NPs carrying anti p53 antibody (p53-PLGA@Au NPs) was 247±108.2 nm. The p53-PLGA@Au NPs had well-defined spherical morphology and hollow interiors observed by electron microscope, and had a good photothermal effect under the irradiation of an 808nm laser. The results of laser scanning confocal microscope (LSCM) and flow cytometer (FCM) indicated the specific targeting of p53-PLGA@Au NPs conjugating with breast cancer MCF-7 cells overexpressing p53 protein in vitro. Also the ultrasound imaging experiments in vitro showed that p53-PLGA@Au NPs were suitable for ultrasound contrast imaging. In conclusion, the p53-PLGA@Au NPs are demonstrated to be novel targeted UCAs and may have potential applications in the early diagnosis and targeted near-infrared (NIR) photothermal therapy of breast cancer in the future.

Keywords: poly(D,L-lactic-co-glycolic acid) nanoparticles; gold nanoshell; anti p53 antibody; targeted ultrasound contrast agents; photothermal therapy

1. Introduction

Breast cancer，which constitutes 25.2% of 14.1 million new cancer cases occurred in 2012 worldwide，is the most common cancer diagnosed and the leading cause of cancer-related deaths in women [1]. Effective prevention of the morbidity and mortality of breast cancer will require the development of new diagnostic and therapeutic strategies aimed at treating early and subclinical disease stages.

Molecular imaging, a noninvasive, real time visualization and measurement of physiological or pathological process in the living organism at the cellular or molecular level [2], can provide a potential tool of earlier detection and accurate diagnosis of breast cancer [3]. Ultrasound (US) imaging has been a primary choice for the diagnosis and evaluation of breast lesions, as it is a safe, real-time measurement, with portable and relatively inexpensive cost [4]. Along with the rapid development of contrast-enhanced ultrasound (CEUS) technology and bio-nanotechnology, a mass of targeted ultrasound contrast agents (UCAs) have emerged [5]. The non-invasive ultrasound molecular imaging enables specific and sensitive depiction of molecular targets with the use of nanoscale targeted UCAs.

At present, the main materials used in the fabrication of UCAs are lipids, proteins and polymers [6]. PLGA, a biocompatible and biodegradable polymer, which has been approved by the FDA and the European Medicine Agency in drug delivery

systems for human use, shows ultrasound contrast-enhancing capabilities [7, 8]. However, , we found that the echo characteristic of UCAs prepared by PLGA was not good enough because of their weak reflection ability[9]. We aim to improve synthesis methods and materials composition for better imaging effect of PLGA.

In addition, it will be of great clinical significance in achieving further ultrasound guided local minimally invasive treatment of breast cancer after early diagnosis via UCAs. Photothermal therapy(PTT) utilizing near-infrared (NIR) lasers and photoabsorbers has drawn increasing attention recently years as an efficient technique for cancer treatment due to its convenience and minimal invasiveness [10]. Gold (Au) nanostructures exhibit good biocompatibility as well as excellent optical and electronic properties, thus allowing the use in biological and medical applications [11, 12, 13]. It has also been reported that Au nanoparticle microcapsules could be used in ultrasound imaging in vivo [14, 15]. The combination of Au nanoshell and polymer for realizing the integration of better imaging diagnosis and photothermal therapy has received worldwide attention. Ke et al [16] prepared a single theranostic agent based on the combination of Au nanoshell and poly (lactic acid) to combine dual modal US/CT contrast imaging diagnosis and photothermal therapy. Kim et al [17] developed methotrexate (MTX)-loaded PLGA, Au/iron (Fe)/Au half-shell nanoparticles, which can be used for magnetic targeted chemo-photothermal treatment. However, those agents cannot be involved in identifying target sites from molecular levels and combine with molecules with high specificity for an appropriately long time because there is no high-affinity binding ligands on the

surface of agent. Furthermore, to our best knowledge, few studies have been conducted to develop targeted Au nanoshelled PLGA nanoparticles for the early diagnosis and targeted photothermal therapy of breast cancer.

The disruption of the p53 pathway is one of the most common genetic alterations in many types of tumors, including those of breast. The p53 tumor suppressor gene (TP53) codes for a 53-kd nuclear phosphoprotein (p53 protein) which has been implicated in controlling cell cycle regulation, cell differentiation, and the surveillance of genomic integrity[18]. The present study [19] suggests that the expression of p53 protein may be an early event in the development of breast cancer. Therefore, p53 protein is a promising target for the diagnosis and treatment of breast cancer.

Thus, this work is aim to develop a nanotheranostic agent that integrates targeted ultrasound imaging and photothermal therapy into one platform for being used in the targeted diagnosis and treatment of breast cancer. In this study, the gold nanoshelled PLGA nanoparticles carrying anti p53 antibody (p53-PLGA@Au NPs), the nanotheranostic agent, was fabricated. And the photothermal effect and the specific targeting with the breast cancer MCF-7 cells were evaluated as novel ultrasound contrast agent in vitro.

2. Experimental

2.1. Materials

Poly (D,L-lactic-co-glycolic acid) (PLGA, carboxylic acid terminated, lactide:

glycolide 50:50, Mw 24,000-38,000) and poly(allylamine hydrochloride) (PAH, Mw~17,500) were purchased from Sigma-Aldrich (Shanghai) Trading Co., Ltd. $HAuCl_4 \cdot 3H_2O$ (Tetrachloroauric (III) acid trihydrate,) was supplied by Acros Organics, USA. Polyvinyl alcohol (PVA, 87-89% mole hydrolyzed, low molecular weight), (D+)-camphor, 1-(3-Dimethylaminopropyl)-3-ethylcarbodiimide hydrochloride (EDC) and N-Hydroxysuccinimide (NHS) were purchased from Aladdin Chemistry Co., Ltd , Shanghai, China). Thiol, Carboxyl -terminated poly (ethylene glycol) (SH-PEG-COOH, Mw 2000) was supplied by Xi'an Ruixi Biological Technology Co., Ltd. Anti p53 antibody (FITC) and anti p53 antibody were obtained from Abcam, USA. All other commercially available chemicals were used as received.

2.2. Preparation of PLGA NPs

PLGA NPs were prepared using an adapted oil-in-water emulsion solvent evaporation process according to previous reports. [20, 21, 22] PLGA (100 mg) and camphor (10 mg) were dissolved in methylene chloride (3.5 mL), and then the O/W emulsion was generated by adding the oil phase dropwise to the PVA aqueous solution (2% w/v, 20 mL).The system was emulsified using an ultrasonic probe in an ice bath and sonicated for 180 seconds Afterwards, the emulsion was stirred at room temperature for 5 h to evaporate the residual methylene chloride. Then the miature was centrifuged and washed with DI water. Finally, the NPs were freeze-dried and filled with C_3F_8 gas.

2.3. Preparation of PLGA@Au NPs

2.3. Preparation of PLGA@Au NPs

Firstly, the citrate-stabilized solution contained Au NPs with diameter of ~6 nm was prepared via a surface seeding method as the previous report.[23, 24] Meanwhile, The PLGA NPs suspension (1 mL) was added in PAH solution (10 mL, 1.0 mg/mL in 0.5 M NaCl aqueous solution) and stirred for 30 min, then centrifuged and washed with DI water. Then the precipitate was suspended into citrate-stabilized Au NPs solution and the centrifuge/wash step was repeated to get the Au NPs coated PLGA NPs. Afterwards, the NPs were re-dispersed and added into $HAuCl_4$ (1% w/v, 2 mL) solution with stirring, then NH_2OH solution (0.3 mL, 0.5 mol/L) was added to reduce of $HAuCl_4$, affording to form Au nanoshell around the PLGA NPs surface.

2.4. Preparation of p53-PLGA@Au NPs

SH-PEG–COOH (5 mg) was added into PLGA@Au NPs aqueous solution, mixed thoroughly and stirring at room temperature for 12 h, then centrifuged and washed by DI water to discard excessive free SH-PEG-COOH molecules. The precipitate was re-dispersed into 2 mL phosphate buffer saline (PBS), then 10 mg NHS and 10 mg EDC were introduced to activate the carboxylic acid groups on the surface of PLGA@Au NPs, and the mixture was stirred gently at room temperature for 1 h, then the centrifuge/wash step was repeated to obtain activated PLGA@Au NPs. [25]Anti p53 antibody or anti p53 antibody with FITC labelled was added into the solution and incubated in thermostatic oscillator for 60 min. Then we got the pure targeted

p53-PLGA@Au NPs by removing the free antibody.

2.5. Characterization

Scanning electron microscope (SEM) images were obtained with S-4800 field emission scanning electron microscope (FE-SEM; Hitachi, Tokyo, Japan), and JEOL JEM-2100 high-resolution transmission electron microscope (HR-TEM; Hitachi) was also used to get the TEM images to observe the morphology and structure of the nanoparticles. The concentration of Au elements in p53-PLGA@Au NPs was determined by inductively coupled plasma atomic emission spectroscopy (ICP-AES, Vistampxicp Varian, USA). The size, polydispersity index (P.I.) and zeta potential of the nanoparticles were measured using a dynamic laser scattering (DLS; Zetasizer Nano ZS3690，Malvern Instruments, Ltd, Malvern, UK). Beckman Coulter DU 730 spectrophotometer was used to evaluate the ultraviolet-visible (UV-vis) absorption spectra of the nanoparticles.

2.6. Biocompatibility

2.6.1. Cell culture

Human breast adenocarcinoma MCF-7 cell line (MCF-7 cells) overexpressing p53 protein and MDA-MB-231 breast cancer cells (231 cells) low-expressing p53 protein (as a control cell line) and human umbilical vein endothelial cells (HUVEC cells) were provided by the Institute of Biochemistry and Cell Biology, SIBS, CAS (China).

They were cultured in Dulbecco's Modified Eagle Medium (DMEM，Gibco Life Technologies, Grand Island, NY, USA) supplemented with 10% fetal bovine serum (FBS) and 1% penicillin-streptomycin, at 37 ℃ under a 5% CO_2 atmosphere.

2.6.2. Toxicity of p53-PLGA@Au NPs

In vitro cytotoxicity was determined by 3-(4,5-Dimethylthiazol-2-yl)-2,5-diphenyltetrazolium bromide (MTT，Solarbio, China) assays on HUVEC and MCF-7 cells. The cells (1×10^4 per well) in 100 μL medium were seeded respectively in a 96-well cell culture plate and were cultured for 24 h. Then the cells were exposed to serial concentrations (0, 10, 20, 50, 100, 200 μg/mL) of the p53-PLGA@Au NPs and further incubated for 12 or 24 h. After removing the medium, 100 μL MTT (0.5 mg/mL) was added to the culture and incubated for additional 4 h at 37°C. Then the culture medium was replaced with 150 μL dimethyl Sulfoxide (DMSO) and the absorbance was measured using a microplate reader (Thermo scientific Multiskan MK3) at the wavelength of 490 nm. The cytotoxicity was expressed as the percentage of cell viability compared with that of untreated control cells.

2.7. Photothermal effect

Photothermal effect of p53-PLGA@Au NPs was assessed via monitoring temperature increase under the laser irradiation. Different concentrations of the agent was suspended in quartz cuvettes (total volume of 1 mL), irradiated by an 808 nm laser

with output power of 1 W for 15 min. The temperature of the solutions was measured by an IR thermal camera. In order to evaluate the thermal stability of the materials, the absorption spectra of the materials was measured before and after the whole process.

In vitro cytoviability assay of p53-PLGA@Au NPs combined with NIR laser was also carried out. MCF-7 cells (1×10^4 per well) were incubated in 96-well plates at 37°C for 24 h. Different dosage (0-200 μg/mL) of p53-PLGA@Au NPs suspensions were added in and incubated with cells for 4 h. Then the cells were irradiated by NIR laser (808nm, 2 W/cm^2) for 8 min and the cell viability was determined by MTT assay. Results are shown as mean ± standard deviation (n = 3).

2.8. Detection the specific targeting of p53-PLGA@Au NPs in vitro

2.8.1. Confocal laser scanning microscopy

MCF-7 and 231 cells at density of 2×10^4 cells per class bottom cell culture dish(Φ =20 mm) were incubated for 12 h and they were respectively divided into three groups as follows, the control group, the targeted group and the targeted inhibition group. MCF-7 and 231 cells in control group were treated with 100 μL PLGA@Au NPs and the cells in the targeted group were treated with 100 μL p53-PLGA@Au NPs for 30 min. For the competition/inhibition studies, 5 μL anti p53 antibody without FITC labelled was added to the incubation medium for 30 min before treated with p53-PLGA@Au NPs. Then cells were washed three times with PBS buffer, fixed with 4% paraformaldehyde for 15 min, and then nuclear stained with the

4,6-diamino-2-phenyl indole (DAPI) solution. Finally, the six samples were evaluated and imaged using a Leica TCS SP5 II laser scanning confocal microscope (LSCM).

2.8.2. Flow cytometry

The groupings were consistent with the LSCM assay. MCF-7 and 231 cells were cultured and treated as previously described. All the cells were centrifuged (1500 rpm, 5 min) after trypsin-digested and the supernatant was discarded in 1 mL sterile PBS and collected in test tubes prior to flow cytometry (FCM) with a density of 2×10^5 cells per tube. All of the experiments mentioned above were repeated three times.

2.9. In vitro US imaging

The preliminary evaluation of the ultrasound contrast behavior of p53-PLGA@Au NPs in vitro was carried out by using Ultrasonic Diagnostic Instrument (L90, Esaote SpA, Genova, Italy) with a 522 transducer. Various concentrations (0-2 mg/mL) of p53-PLGA@Au NPs were dispersed in the degassed deionized water in tubes (2 mL) and pure degassed deionized water was injected in the same tube to serve as background control. The comparison of imaging ability of p53-PLGA@Au NPs and PLGA NPs was also carried out simultaneously. The samples were scanned using the transducer in contrast mode (mechanical index, MI=0.10, the range of frequency was 3-9 MHz) in a tank filled with degassed deionized water.

2.10. Statistical analysis

Results are presented as the mean ± standard deviation. Student's t-test was utilized to identify the significance of differences between the experimental and control groups using SPSS, version 17.0 (SPSS, Inc., Chicago, IL, USA). $P<0.05$ was considered to indicate a statistically significant difference.

3. Results and discussion

3.1. Characterization of nanoparticles

The structure of p53-PLGA@Au NPs is well illustrated in Figure 1. In our synthesis, the polymeric nanoparticles provide the hollow core which could be a basis for the ultrasound-responsive properties and a dielectric interface for shifting the plasmon resonance of the gold nanoshells to the NIR wavelength region. [8, 20] The Au nanoshell on the outer surface can enhance the reflection of the agents, and be heated by NIR lasers as photoabsorbers in photothermal therapy. And anti p53 antibody was the targeted moiety to target p53 protein expressing in MCF-7 breast cancer cells.

The PLGA NPs were firstly synthesized using the O/W synthetic process. SEM image (Figure 2(a)) revealed the spherical morphology of the well dispersed PLGA NPs. Some cavities could be observed in our NPs as indicated by the arrows. To clearly observe the hollow interiors of the PLGA NPs via TEM, the freshly prepared phosphate solution (1%, W/V) was used when the NPs were dispersed onto the copper coated carbon diaphragm. As shown in Figure 2(b), the hollow interiors of

the PLGA NPs making by the camphor sublimation and the collapse of the NPs were clearly demonstrated. Figure 2e is a partial magnified image, displaying the hollow interior structure of the PLGA NPs. It is believed that the hollows of the NPs arose from the evacuation procedure performed during SEM and TEM operation, which inevitably led to the NPs' collapse. The PLGA NPs with an average diameter of 228.8±60.4 nm have a negative surface charge, which could easily adsorb positively charged PAH for subsequent attachment of negative charged citrate-stabilized Au NPs. The attached 5~7 nm Au NPs were used as seeds, allowing $HAuCl_4$ added to form the Au coating around the PLGA NPs surface by a seeding procedure.

The targeted p53-PLGA@Au NPs was synthesized by using SH-PEG-COOH as an intermediate to connect antibodies and PLGA@Au NPs. Thiol and Au element of PLGA@Au NPs can tight junctions through Au-S linkage. And the classical EDC/NHS method[26] was used to activate the carboxylic acid groups of PEGylated PLGA@Au NPs to combine with the amino groups of antibodies via covalent interactions, forming a durable layer that serves as targeted agents.

Figure 2(c) and 2(d) display the SEM and TEM images of p53-PLGA@Au NPs. Au NPs could be clearly observed on the rough surface of p53-PLGA@Au NPs from the SEM and TEM images, indicating the gold nanoshell formed successfully. In comparison with PLGA NPs, the aggregated gold nanoparticles developed slightly rough surfaces and made the mean size of the NPs further increase from 228 to 247 nm (Figure 3(a)). The low polydispersity index value (P.I. = 0.127) of p53-PLGA@Au NPs suggests a narrow distribution and high homogeneity in size,

and the zeta potential was -34.2±5.8 mV (Figure 3(b)), implying the solution has good stability. The diameter and zeta potentials of p53-PLGA@Au NPs solutions changed little($P>0.05$) as the time elapses (0 h, 0.5 h, 1 h, 6 h, 12 h), which also indicates the good stability of NPs (Table. 1) The amount of Au element in p53-PLGA@Au NPs was 60.5 % in weight. The result suggests the existence of Au nanoshells and provides the evidence to measure the concentration of PLGA in p53-PLGA@Au NPs accurately in ultrasound contrast imaging assay in vitro.

In addition, Figure 4(a) shows the UV-Vis-NIR absorption spectra of samples at different preparation stages, including PLGA NPs, Au NPs, PLGA@Au NPs and p53- PLGA@Au NPs. The PLGA NPs shows no obvious peak in the range from 400 nm to 900 nm in the spectrum while the Au NPs have maximum absorption peak at 522 nm. Both of the PLGA NPs and Au NPs have no obvious absorption in NIR region. But a continuous broad peak ranging from 500 to 900 nm can be observed from PLGA@Au NPs absorption spectra. It could be attributed to the seeding process, which made the attached gold nanoparticles on the PLGA NPs surface grow larger and more enough leading to NIR absorption. The broad peak in NIR region of p53-PLGA@Au NPs confirms the ability as photoabsorbers for NIR photothermal ablation therapy.

3.2. Photothermal effect

Under the irradiation of NIR laser, we verified the photothermal capability of p53-PLGA@Au NPs suspensions by monitoring temperature increase. It could be

observed that the temperature of the solution was rapidly increased when laser is on for 15 min (figure 4(b)). In detail, the temperature increase was 11 °C when the concentration reached up to 0.2 mg/ mL, while there was only less than 1 °C increase for the DI water itself. The obviously difference illustrated that the NPs suspension at a relatively low concentration could be easily heated up to above 42 °C accompanying with the irradiation of the NIR light, which can meet the temperature of kill tumor cells. To determine the stability of p53-PLGA@Au NPs when exposing in the irradiation of NIR laser, we collected the UV-Vis-NIR absorption spectra of samples at the beginning and ending of the assay. The graphs shown in Figure 4(c) clearly confirms the p53-PLGA@Au NPs aqueous solution kept still in consistent with the beginning absorption spectrum after the irradiation of NIR laser, ensuring p53-PLGA@Au NPs as the efficient photoabsorbers.

To evaluate the photothermal effect of p53-PLGA@Au NPs in vitro, MCF-7 cells incubated with p53-PLGA@Au NPs suspension of different concentrations (0, 50, 100, 150, 200 μg/mL) for 4 h were irradiated with and without NIR laser for 8 min and then monitored the cells viabilities by MTT assay. The cell viability without NIR light irradiation were 90.4%, 86.8%, 88.1%, 84.6% with 50, 100, 150, 200 μg/mL (Figure 4(d)), implying that the agent itself had little impact on cell survival. And when only laser without materials (dosage=0 μg/mL), there were more than 80% viable cells, demonstrating laser only has no obvious effect on cell survival. On the contrary, while the MCF-7 cells were treated with laser irradiation，there was a significant decrease of cell viabilities accompanied by the increasing concentration of

p53-PLGA@Au NPs. When the concentration of NPs was 200 μg/mL, only less than 20% of the MCF-7 cells remained viable. All those prove that the p53-PLGA@Au NPs is a potential candidate for photothermal therapy.

3.3. In vitro cytotoxicity

The biocompatibility of NPs, which is one of primary concerns in using the NPs as promising potential biomedical materials for future cell experiments and in vivo applications, should be identified first. Thus, MTT assays were used to study the cytotoxicity effect of p53-PLGA@Au NPs in tumor cell line (MCF-7 cells) and non-tumor cell line (HUVEC cells). As shown in the Figure 5(a, b), the cells after 24 h of incubation remained more than 90% of viability even in 200 μg/mL dosage, which illustrates that the p53-PLGA@Au NPs exhibits little cytotoxicity to these two cell lines, indicating the good biocompatibility of p53-PLGA@Au NPs, which could ensure safety for further ultrasound imaging and clinical cancer therapeutics.

3.4. Detection the specific targeting of p53-PLGA@Au NPs in vitro

3.4.1. Confocal laser scanning microscopy

Fluorescein isothiocyanate (FITC) is a widely used fluorescence labeling reagent. It can easily bind several kinds of monoclonal antibodies, so it is served as a green fluorescence probe for immune detection, fluorescence microscopy and flow cytometry. Unlike previous reports [27, 28], we chose antibody-labelled FITC fluorescence, and the connection of NPs and antibody could be observed more simply

and visually by LSCM. As shown in Figure 6, both PLGA@Au NPs (Figure 6(a1)) and p53-PLGA@Au NPs (Figure 6(b1)) can be observed in bright field. And the p53-PLGA@Au NPs shows a bright green fluorescence, indicating the conjugation of anti p53 antibody to the surface of NPs (Figure 6(b2)), while PLGA@Au NPs shows no fluorescence signal (Figure 6(a2)). The results imaged by fluorescence microscopy confirm that anti p53 antibody was immobilized on p53-PLGA@Au NPs.

In order to ensure the accuracy of selection of target cell line which is used for the specific targeting assay of NPs in vitro, the expression of p53 protein in MCF-7 cells was determined by Western Blotting. Briefly, supernatant protein of MCF-7 cells was loading to sodium dodecyl sulfate polyacrylamide gel electrophoresis (SDS-PAGE) and transferred to polyvinylidene fluoride membranes (PVDF). After separating, imaging and documenting the protein separation gel, the expression band was visualized. Figure 6(c) clearly shows the certain band position on the protein separation gel and confirms the expression of p53 protein in MCF-7 cells. The result provides the evidence of choosing MCF-7 cells as targeted cells to evaluate the specific targeting of p53-PLGA@Au NPs in vitro.

We utilized LSCM to confirm the targeted capability qualitatively of p53-PLGA@Au NPs in vitro. It can be seen from Figure 7(a) that MCF-7 cells incubated with p53-PLGA@Au NPs show bright green fluorescence signals. On the contrary, negligible fluorescence is detected in the non-targeted PLGA@Au NPs treated MCF-7 cells (Figure 7(b)) and the MCF-7 cells (Figure 7(c)), which were pre-treated with excess free anti p53 antibody and then incubated with

p53-PLGA@Au NPs. The results demonstrate that the p53-PLGA@Au NPs have the capability of targeting, and the behavior is receptor-mediated through the combination of p53-PLGA@Au NPs and p53 receptors on the MCF-7 cells. In addition, little fluorescence is observed when 231 cells incubated with p53-PLGA@Au NPs under similar conditions like targeted group (Figure 7(d)), indicating that P53-PLGA@Au NPs binds to MCF-7 cells overexpressing P53 receptors more efficiently. In order to clearly express the internalization of the NPs and cells, we provide the bright field image (a1) and the overlay image (a2,). The black spots were the NPs, and they distributed on the cell surface as well as in the cells cytoplasm.

3.4.2. Flow cytometry

The targeting rate of p53-PLGA@Au NPs conjugating toward cells was further assessed quantitatively via FCM. Clearly, as illustrated in Figure 7, MCF-7 cells incubated with p53-PLGA@Au NPs (Figure 7(e)) show remarkably higher fluorescence signals (73±5.21% positively labeling cells) compared with 231 cells (Figure 7(h)) incubated with the same NPs (2.21±0.45% positively labeling cells, $P<0.05$). We can also find that MCF-7 cells in the control NPs group (Figure 7(f)) and the targeted inhibition group (Figure 7(g)) were not positively labelled.

Results all above reveal the specific targeting of p53-PLGA@Au NPs. Therefore, the qualitative targeted behavior was visually verified by LSCM images and the FCM results provide further strong evidence that p53-PLGA@Au NPs have

targeting ability of recognizing and combining with the MCF-7 cells, which are known in overexpressing p53 protein.

3.5. In vitro ultrasound imaging

The capability of targeted p53-PLGA@Au nanoparticles as a contrast agent for ultrasound imaging was assessed in vitro using the My Lab L90 scanner system at various concentrations. Observed from US contrast-enhanced images in Figure 8(a), the tubes filled with p53-PLGA@Au NPs displayed a strong dotted echo in both two-dimensional (2D) and CEUS images, whereas the tube filled with degassed deionized water was observed as anecho. Although the ultrasound signals gradually decreased with decreasing concentrations of p53-PLGA@Au NPs, the signal intensity remained relatively strong at the low concentration of 0.1 mg/mL.

To verify the signal intensity of the different concentrations of p53-PLGA@Au NPs quantitatively, comparative analysis was conducted using QontraXt V3.06 software which can provide the time-intensity curve (TIC) quantitative information. As indicated in Figure 8(a), the p53-PLGA@Au NPs at 2 mg/mL had a higher contrast enhancement effect compared with that of NPs at 0.1 mg/mL (45.4±3.2 dB vs. 86.2±1.8 dB, $P<0.05$), which may be due to the higher back scattering of the former. Thus, the TIC keep correspondence with the visual observation, and such contrast enhancement is also concentration-dependent.

Furthermore, the length of imaging time in vitro of p53-PLGA@Au NPs was pursued at the concentration of 2 mg/mL. Figure 8(b) showed that p53-PLGA@Au

NPs had satisfactory contrast enhancement signal before 4 min and the echo signal strength of agent weakened gradually with time elapsing. It is notable that the signal enhancement can also be obviously observed even after eight minutes of the administration, and the length of imaging time can satisfy the requirement of time of clinical contrast-enhanced ultrasonography.

To explore whether Au nanoshell can enhance ultrasound imaging or not, the imaging comparative study of PLGA and p53-PLGA@Au NPs was carried out in the case of maintaining consistency of PLGA concentration (0.5 mg/mL) according to the result of ICP values of the Au element in the p53-PLGA@Au NPs. The p53-PLGA@Au NPs had higher dotted echo than PLGA NPs, and TIC also verified it. (75.4±2.4 vs. 45.5±3.1, $P<0.05$), as shown in Figure 9(a). In order to confirm detachment of antibody and Au NPs from the PLGA nanoparticles, the size, zeta potential and the UV-Vis-NIR absorption spectra of p53-PLGA@Au NPs were measured before and after the ultrasound imaging process. The results (figure 9b-d) showed that there was no appreciably change over the imaging process. The reason is probably that gold nanoshell with high atomic number and density on the surface of p53-PLGA@Au NPs plays a role in providing stronger backscattering in ultrasound imaging.

We found that the formation of gold nanoshell on the surface of p53-PLGA@Au NPs can improve its ultrasound contrast enhancing capability. And we also made a quantitative analysis of the intensity of the ultrasound imaging, providing more quantitative information by TIC. Importantly, compared with

previous studies [16, 22, 29], we successfully combined the NPs with anti p53 antibody, making the NPs as a candidate nanotheranostic agent for targeted ultrasound molecular imaging and photothermal therapy of breast cancer. However, in the preparation process, there are some subsequent steps after C_3F_8 gas filled in PLGA NPs, it is difficult to assess the actual loading of the gas at the resulting agent.

4. Conclusion

In summary, p53-PLGA@Au NPs, a nanotheranostic agent integrating ultrasound imaging with photothermal therapy has been designed, fabricated and evaluated in vitro. In our study, we developed uniform nano-sized targeted PLGA@Au NPs which are small enough to leak through the pores of tumor vessels. The targeting capability of our NPs conjugating with breast cancer MCF-7 cells overexpressing p53 protein was verified in vitro via LSCM and FCM. The imaging results demonstrate that p53-PLGA@Au NPs provided excellent contrast enhancement for ultrasound imaging and the formation of gold nanoshell enhanced the imaging effect. The resulting NPs also served as efficient photoabsorbers for NIR photothermal therapy. Therefore, the p53-PLGA@Au NPs has potential applications as novel targeted UCAs and photoabsorbers for the theranostic of breast cancer. Further study is still required to verify the targeted ultrasound molecular imaging and photothermal effect of p53-PLGA@Au NPs in vivo, and much more quantitative analysis is needed.

Acknowledgments

The present study was supported by the National Natural Science Foundation of China under Grant [number 81571678]; the Natural Science Foundation of Shanghai under Grant [number 15ZR1425600]; the Natural Science Foundation of Shanghai under Grant [number 14411968200]; and the Transverse Project of Renji Hospital, School of Medicine, Shanghai Jiao Tong University under Grant [number RJKY14-07].

References

1. Ferlay J, Soerjomataram I, Dikshit R, Eser S, Mathers C, Rebelo M, Parkin DM, Forman D, Bray F. Cancer incidence and mortality worldwide: sources, methods and major patterns in GLOBOCAN 2012. International journal of cancer. 2015;136:E359-86.
2. Chen ZY, Wang YX, Lin Y, Zhang JS, Yang F, Zhou QL, Liao YY. Advance of molecular imaging technology and targeted imaging agent in imaging and therapy. BioMed research international. 2014;2014:819324.
3. Bachawal SV, Jensen KC, Lutz AM, Gambhir SS, Tranquart F, Tian L, Willmann JK. Earlier detection of breast cancer with ultrasound molecular imaging in a transgenic mouse model. Cancer research. 2013;73:1689-98.
4. Funke M. Diagnostic imaging of breast cancer : An update. Der Radiologe. 2016.
5. Yang F, Chen ZY, Lin Y. Advancement of targeted ultrasound contrast agents and their applications in molecular imaging and targeted therapy. Current pharmaceutical design. 2013;19:1516-27.
6. Wen Q, Wan S, Liu Z, Xu S, Wang H, Yang B. Ultrasound contrast agents and ultrasound molecular imaging. Journal of nanoscience and nanotechnology. 2014;14:190-209.
7. Lavisse S, Paci A, Rouffiac V, Adotevi C, Opolon P, Peronneau P, Bourget P, Roche A, Perricaudet M, Fattal E, Lassau N. In vitro echogenicity characterization of poly[lactide-coglycolide] (plga) microparticles and preliminary in vivo ultrasound enhancement study for ultrasound contrast agent application. Investigative radiology. 2005;40:536-44.
8. Lv J-M, Wang x, Marin-Muller C, Wang H, Lin PH, Yao Q, Chen C. Current advances in research and clinical applications of PLGA based nanotechnology. Expert Reviews. 2009;9:325-41.
9. Cui W, Bei J, Wang S, Zhi G, Zhao Y, Zhou X, Zhang H, Xu Y. Preparation and

evaluation of poly(L-lactide-co-glycolide) (PLGA) microbubbles as a contrast agent for myocardial contrast echocardiography. Journal of biomedical materials research Part B, Applied biomaterials. 2005;73:171-8.
10. Song J, Qu J, Swihart MT, Prasad PN. Near-IR responsive nanostructures for nanobiophotonics: emerging impacts on nanomedicine. Nanomedicine : nanotechnology, biology, and medicine. 2016;12:771-88.
11. Jabeen F, Najam-ul-Haq M, Javeed R, Huck CW, Bonn GK. Au-nanomaterials as a superior choice for near-infrared photothermal therapy. Molecules (Basel, Switzerland). 2014;19:20580-93.
12. Jiang Y, Fei W, Cen X, Tang Y, Liang X. Near-infrared Light Activatable Multimodal Gold Nanostructures Platform: An Emerging Paradigm for Cancer Therapy. Current cancer drug targets. 2015;15:406-22.
13. Shanmugam V, Selvakumar S, Yeh CS. Near-infrared light-responsive nanomaterials in cancer therapeutics. Chemical Society reviews. 2014;43:6254-87.
14. Arifin DR, Long CM, Gilad AA, Alric C, Roux S, Tillement O, Link TW, Arepally A, Bulte JW. Trimodal gadolinium-gold microcapsules containing pancreatic islet cells restore normoglycemia in diabetic mice and can be tracked by using US, CT, and positive-contrast MR imaging. Radiology. 2011;260:790-8.
15. Kim J, Arifin DR, Muja N, Kim T, Gilad AA, Kim H, Arepally A, Hyeon T, Bulte JW. Multifunctional capsule-in-capsules for immunoprotection and trimodal imaging. Angewandte Chemie. 2011;50:2317-21.
16. Ke H, Yue X, Wang J, Xing S, Zhang Q, Dai Z, Tian J, Wang S, Jin Y. Gold nanoshelled liquid perfluorocarbon nanocapsules for combined dual modal ultrasound/CT imaging and photothermal therapy of cancer. Small. 2014;10:1220-7.
17. Kim HJ, Lee SM, Park KH, Mun CH, Park YB, Yoo KH. Drug-loaded gold/iron/gold plasmonic nanoparticles for magnetic targeted chemo-photothermal treatment of rheumatoid arthritis. Biomaterials. 2015;61:95-102.
18. Royds JA, Iacopetta B. p53 and disease: when the guardian angel fails. Cell death and differentiation. 2006;13:1017-26.
19. Milicevic Z, Bajic V, Zivkovic L, Kasapovic J, Andjelkovic U, Spremo-Potparevic B. Identification of p53 and its isoforms in human breast carcinoma cells. TheScientificWorldJournal. 2014;2014:1-10.
20. Ke H, Wang J, Tong S, Jin Y, Wang S, Qu E, Bao G, Dai Z. Gold nanoshelled liquid perfluorocarbon magnetic nanocapsules: a nanotheranostic platform for bimodal ultrasound/magnetic resonance imaging guided photothermal tumor ablation. Theranostics. 2013;4:12-23.
21. WANG C-W, YANG S-P, HU H, DU J, LI F-H. Synthesis, characterization and in vitroand in vivo investigation ofC3F8-filled poly(lactic-co-glycolic acid) nanoparticles as an ultrasound contrast agent. Molecular medicine reports. 2014;00.
22. Ke H, Wang J, Dai Z, Jin Y, Qu E, Xing Z, Guo C, Yue X, Liu J. Gold-nanoshelled microcapsules: a theranostic agent for ultrasound contrast imaging and photothermal therapy. Angewandte Chemie. 2011;50:3017-21.
23. Jin Y, Wang J, Ke H, Wang S, Dai Z. Graphene oxide modified PLA

microcapsules containing gold nanoparticles for ultrasonic/CT bimodal imaging guided photothermal tumor therapy. Biomaterials. 2013;34:4794-802.
24. Jing L, Liang X, Li X, Lin L, Yang Y, Yue X, Dai Z. Mn-porphyrin conjugated Au nanoshells encapsulating doxorubicin for potential magnetic resonance imaging and light triggered synergistic therapy of cancer. Theranostics. 2014;4:858-71.
25. Wu H, Shi H, Zhang H, Wang X, Yang Y, Yu C, Hao C, Du J, Hu H, Yang S. Prostate stem cell antigen antibody-conjugated multiwalled carbon nanotubes for targeted ultrasound imaging and drug delivery. Biomaterials. 2014;35:5369-80.
26. Liu J, Li J, Rosol TJ, Pan X, Voorhees JL. Biodegradable nanoparticles for targeted ultrasound imaging of breast cancer cells in vitro. Physics in medicine and biology. 2007;52:4739-47.
27. Kohl Y, Kaiser C, Bost W, Stracke F, Fournelle M, Wischke C, Thielecke H, Lendlein A, Kratz K, Lemor R. Preparation and biological evaluation of multifunctional PLGA-nanoparticles designed for photoacoustic imaging. Nanomedicine : nanotechnology, biology, and medicine. 2011;7:228-37.
28. Yang H, Cai W, Xu L, Lv X, Qiao Y, Li P, Wu H, Yang Y, Zhang L, Duan Y. Nanobubble-Affibody: Novel ultrasound contrast agents for targeted molecular ultrasound imaging of tumor. Biomaterials. 2015;37:279-88.
29. Xi J, Qian X, Qian K, Zhang W, He W, Chen Y, Han J, Zhang Y, Yang X, Fan L. Au nanoparticle-coated, PLGA-based hybrid capsules for combined ultrasound imaging and HIFU therapy. J Mater Chem B. 2015;3:4213-20.

Table 1. Stability of p53-PLGA@Au NPs ($\bar{x}\pm S$).

Figure 1. Schematic diagram of p53-PLGA@Au NPs.

Figure 2. SEM (scale=2 μm) and TEM (scale=200 nm) of PLGA NPs (a, b) and p53-PLGA@Au NPs(c, d); SEM of the cross-section of PLGA NPs (e).

Figure 3. (a) Size distribution and (b) Zeta potential of p53-PLGA@Au NPs.

Figure 4. (a) UV-Vis-NIR absorption spectra of the NPs at different stages of fabrication process; (b) temperature increase (laser on) and decrease (laser off) of water (control) and p53-PLGA@Au NPs with different concentrations irradiated by an 808 nm NIR laser with output power of 1 W; (c) UV-Vis-NIR absorption spectrum at the beginning and ending of the solution photothermal effect assay;(d) Cell

viabilities of MCF-7 cells incubated with p53-PLGA@Au NPs at different dosages (0, 50, 100,150, 200 μg/mL) with or without NIR laser irradiation (808 nm, 2 W/cm^2, 8 min, data expressed as mean ± s.d.)

Figure 5. Cell viabilities of (a) HUVEC cells and (b) MCF-7 cells at different dosages of the p53-PLGA@Au NPs (0, 10, 20, 50, 100, 200 μg/mL, data expressed as mean ± s.d.).

Figure 6. Confocal microscopic images of PLGA@Au NPs (a1, a2) and p53-PLGA@Au NPs (b1,b2) with 63 oil-immersion lens , (a1,b1) are the bright field images and (a2,b2) are the FITC fluorescence images;(c) the expression of p53 protein of MCF-7 cells via Western Blotting.

Figure 7. Confocal microscopic images and flow cytometry results of MCF-7 cells incubated with p53-PLGA@Au NPs (a/a1-a4, e) and PLGA@Au NPs (b, f), free p53 antibody pre-treated MCF-7 cells incubated with p53-PLGA@Au NPs (c, g), and 231 cells incubated with p53-PLGA@Au NPs (d, h).

Figure 8. (a) In vitro two-dimensional (2D) and contrast-enhanced ultrasound (CEUS) images and the time-intensity curves (TIC) of p53-PLGA@Au NPs at different concentrations. (b) In vitro US images of p53-PLGA@Au NPs at various imaging times (concentration=2 mg/mL)

Figure 9. (a) In vitro two-dimensional (2D) and contrast-enhanced ultrasound (CEUS) images and the time-intensity curves (TIC) of p53-PLGA@Au NPs and PLGA NPs with the same PLGA concentration (0.5 mg/mL); The diameter (b), zeta potentials (c)

and UV-Vis-NIR absorption spectra (d) of p53-PLGA@Au NPs solutions measured before and after the ultrasound imaging process.

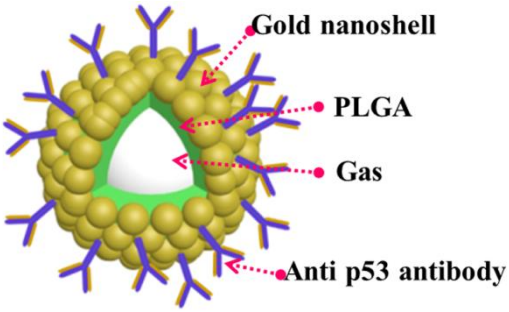

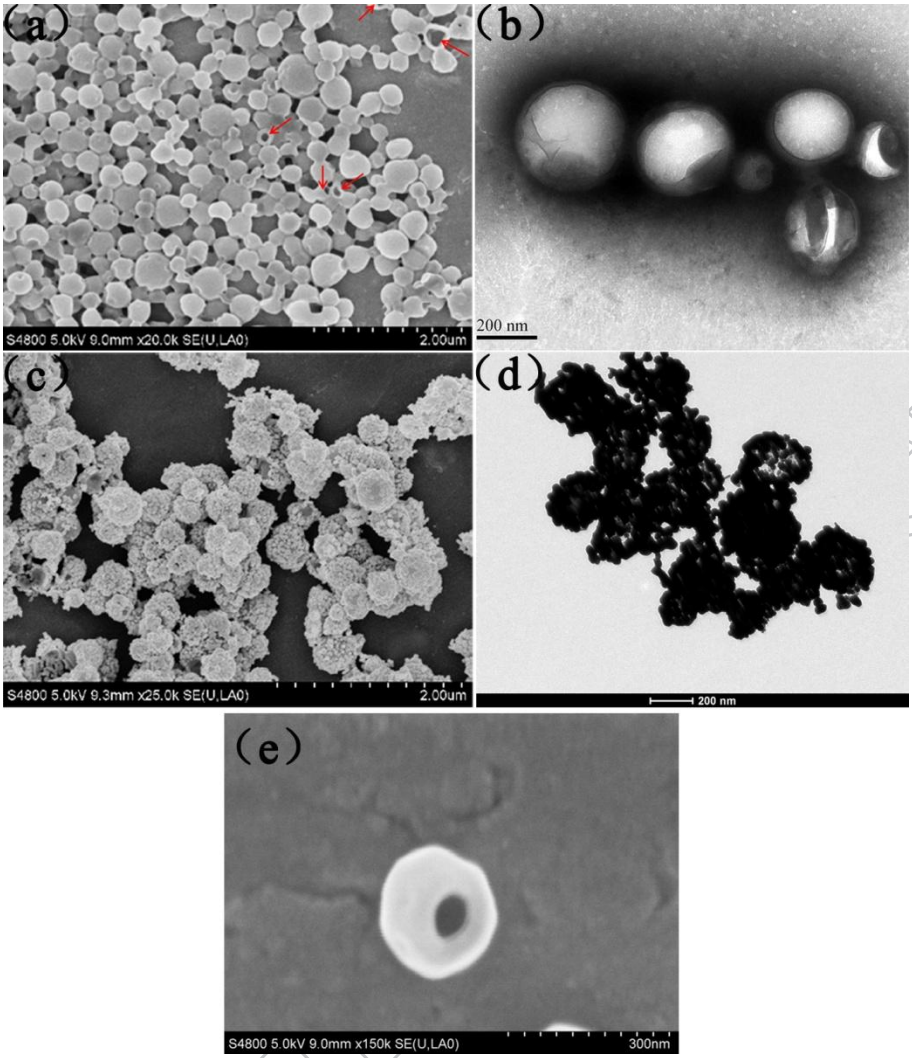

(a)

		Size (d.n...	% Intensity	Width (d.n...
Z-Average (d.nm): 247.7	Peak 1:	283.9	100.0	108.2
PdI: 0.127	Peak 2:	0.000	0.0	0.000
Intercept: 0.896	Peak 3:	0.000	0.0	0.000
Result quality Good				

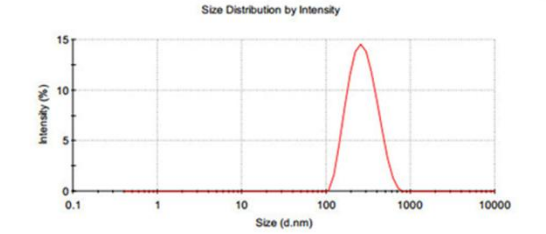

(b)

		Mean (mV)	Area (%)	Width (mV)
Zeta Potential (mV): -34.2	Peak 1:	-34.2	100.0	5.85
Zeta Deviation (mV): 5.85	Peak 2:	0.00	0.0	0.00
Conductivity (mS/cm): 0.00514	Peak 3:	0.00	0.0	0.00
Result quality Good				

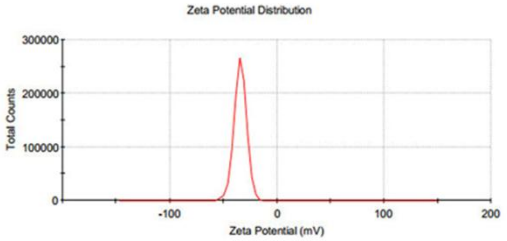

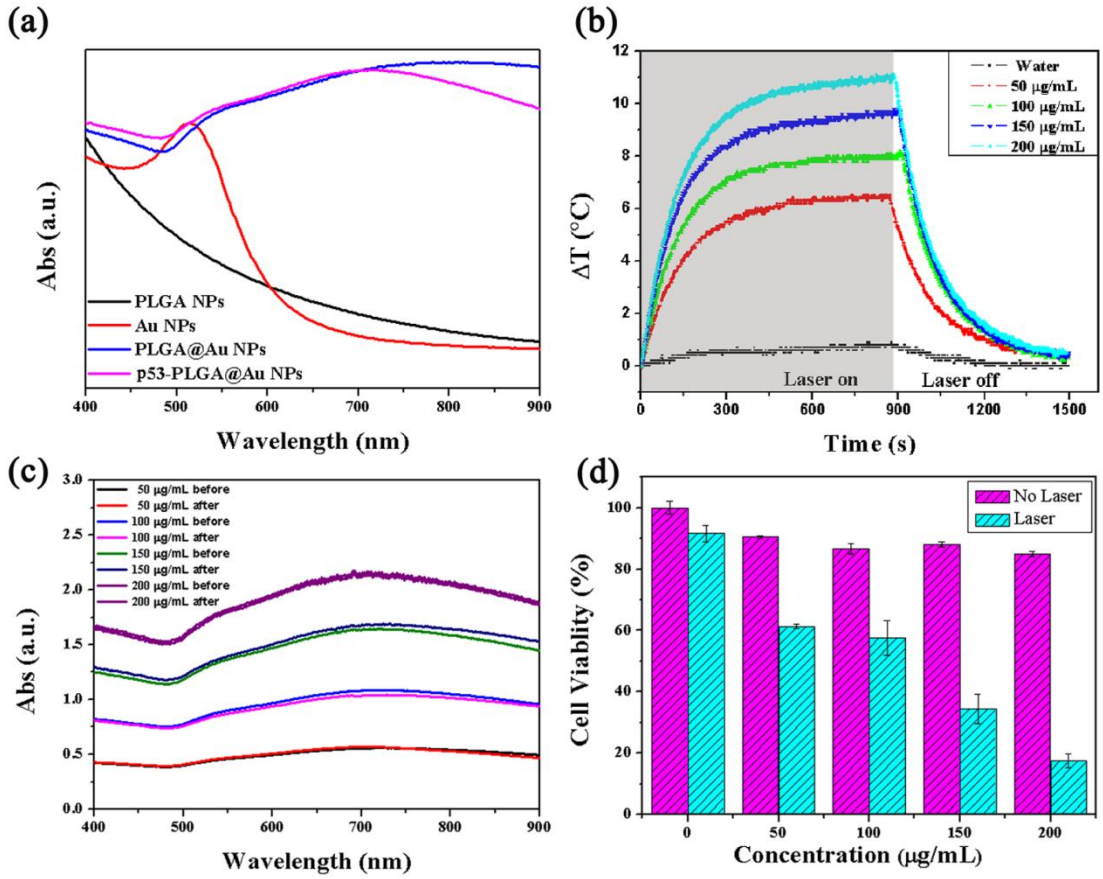
(a)
Abs (a.u.)
PLGA NPs
Au NPs
PLGA@Au NPs
p53-PLGA@Au NPs
Wavelength (nm)
(b)
ΔT (°C)
Water
50 μg/mL
100 μg/mL
150 μg/mL
200 μg/mL
Laser on
Laser off
Time (s)
(c)
Abs (a.u.)
50 μg/mL before
50 μg/mL after
100 μg/mL before
100 μg/mL after
150 μg/mL before
150 μg/mL after
200 μg/mL before
200 μg/mL after
Wavelength (nm)
(d)
Cell Viablity (%)
No Laser
Laser
Concentration (μg/mL)

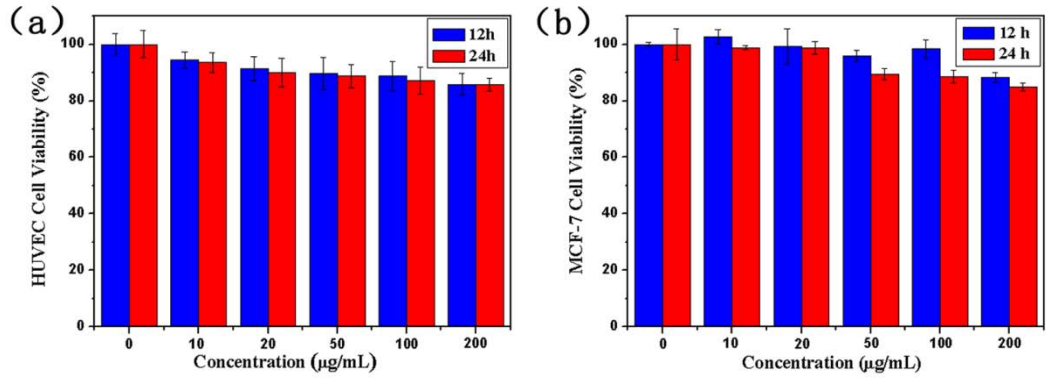

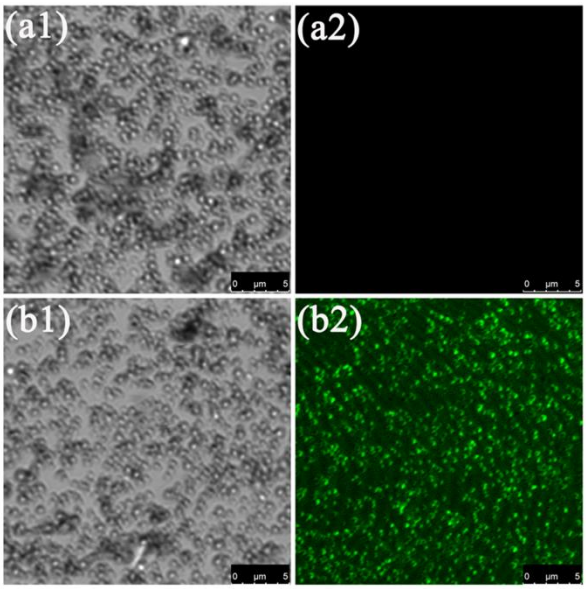

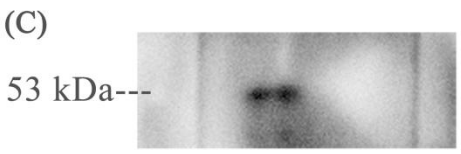

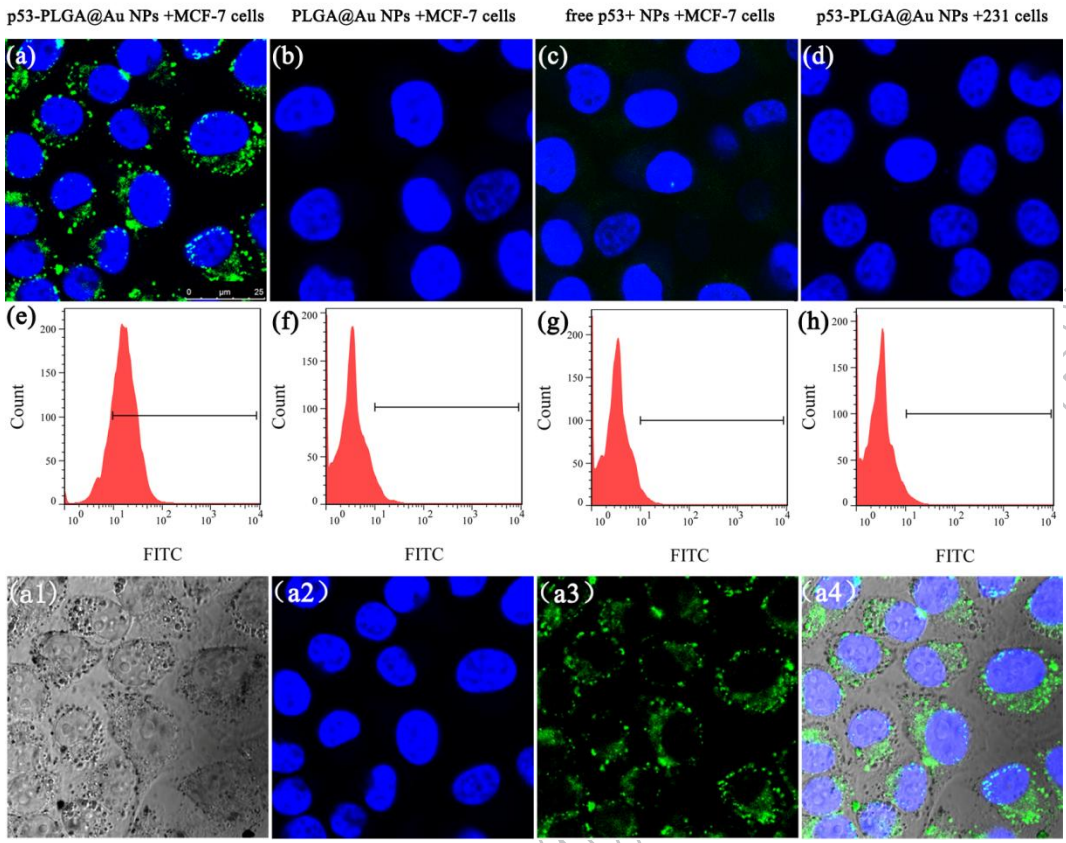

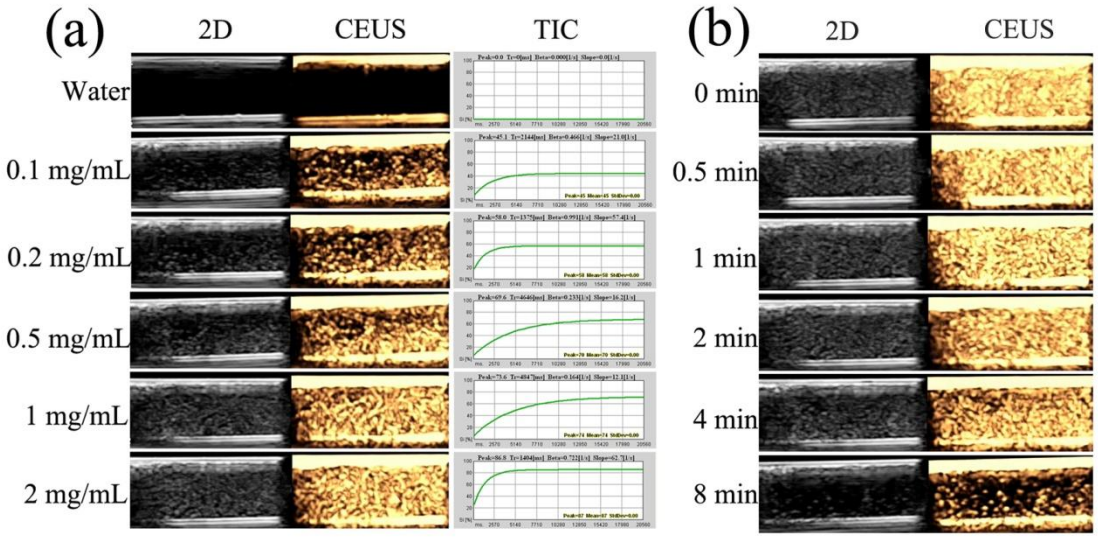

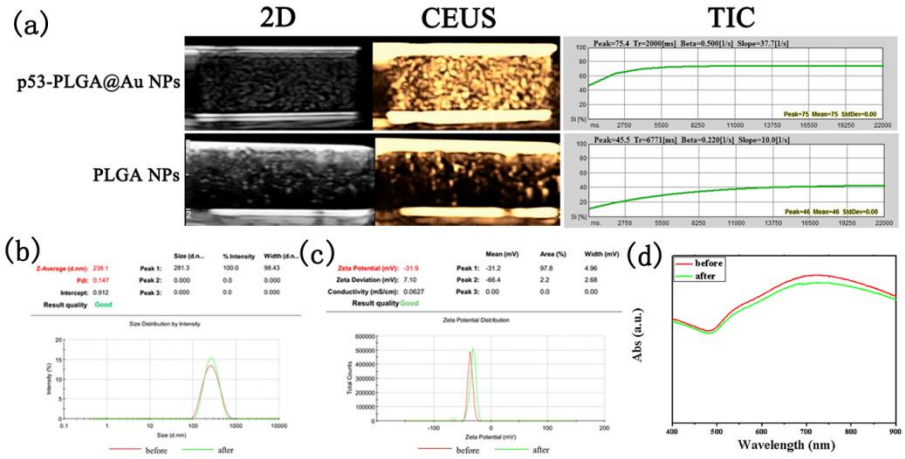

Table

Table.1 Stability of p53-PLGA@Au NPs ($\bar{x}$±S)

p53-PLGA@Au NPs	0 h	0.5 h	1 h	6 h	12 h
Diameter (nm)	247.7±108.2	253.7±79.2	259.8±89.4	263.7±98.5	270.8±77.6
Zeta potential (mV)	-34.2±5.85	-31.6±8.85	-30.5±7.99	-32.2±6.43	-27.2±9.63

No significant statistical differences between groups（P>0.05）.